Optics Letters

2D beam shaping via 1D spatial light modulator using static phase masks

JAMES E. M. WHITEHEAD,[1] ALBERT RYOU,[1] SHANE COLBURN,[1] MAKSYM ZHELYEZNYAKOV,[1]
AND ARKA MAJUMDAR[1,2,*]

[1]*Department of Electrical and Computer Engineering, University of Washington, Seattle, Washington 98195, USA*
[2]*Department of Physics, University of Washington, Seattle, Washington 98195, USA*
*Corresponding author: arka@uw.edu

Many emerging, high-speed, reconfigurable optical systems are limited by routing complexity when producing dynamic, two-dimensional (2D) electric fields. We propose a gradient-based inverse-designed, static phase-mask doublet to generate arbitrary 2D intensity wavefronts using a one-dimensional (1D) intensity spatial light modulator (SLM). We numerically simulate the capability of mapping each point in a 49 element 1D array to a distinct 7 × 7 2D spatial distribution. Our proposed method will significantly relax the routing complexity of electrical control signals, possibly enabling high-speed, sub-wavelength 2D SLMs leveraging new materials and pixel architectures. © 2021 Optical Society of America

Fast, dynamic manipulation of two-dimensional (2D) optical fields is integral to many emerging applications, including optical holography [1], non-line-of-sight imaging [2], optical neural networks [3,4] and imaging through disorder [5]. Currently, most of these applications rely on either digital micromirror devices or liquid crystal-based spatial light modulators (SLMs). Both technologies suffer from low-speed operation ($\sim 1-100$ kHz), due to large inertia and high-power consumption of the liquid crystals or mechanical mirrors. Many of the aforementioned applications, however, require much higher-speed (~ 100 MHz-1 GHz) modulation. Field-induced electro-optic modulation via free-carrier dispersion [6] or the Pockels effect [7], can potentially increase the speed by several orders of magnitude, as evidenced by their use in high-speed optical interconnects. An increase in operating speed, however, must be accompanied by a reduction in switching energy per pixel (E_{sw}) to maintain an acceptable level of power consumption. For an SLM with N number of pixels operating at a frequency of f_o, the total operating power becomes $\sim E_{sw} N f_o$. For a field-induced modulation method, the switching energy is directly proportional to the active pixel volume V_m. Maintaining this switching energy at an acceptable level requires $V_m < \lambda^3$, λ being the operating wavelength and is largely independent of the reconfiguration mechanism being used [8]. Such a sub-wavelength volume also necessitates the pixel separation to be sub-wavelength. Unfortunately, accommodating a high pixel

count 2D SLM with a sub-wavelength pitch poses a significant challenge in terms of the routing of electrical control wires. A 2D SLM with $N \times N$ pixels will need N^2 control signals with an electrode spacing of $\sim \lambda/N$ to address all pixels along each row. At visible wavelengths, where each phase shifter has its own pair of electrical contacts, the most sophisticated semiconductor fabrication techniques cannot exceed $N \sim 10$. While using vias (out-of-plane wires connecting conductors in different layers in semiconductor fabrication), we can exploit multi-layers of metallic interconnects, and a prohibitively large number of vias will be needed to scale the number of pixels to the state-of-the-art values ($\sim 10^5-10^6$). The number of control signals can be reduced to $O(N)$ by exploiting active electronics, including a thin film transistor-based active matrix. While such active electronics are a norm in displays (speed of ~ 100 frames per second), realizing high-speed operation (~ 100 MHz, i.e., $\sim 10^8$ frames per second) using active matrix is very difficult, even for a modest number of pixels [9]. $O(N)$ signals to control N^2 pixels can also be realized, if the changed state of the pixels can be held without an external signal for a sufficiently long time to be periodically refreshed. Unfortunately, most field-induced electro-optic effects are volatile and disappear very soon after the control is removed.

A 1D SLM, however, is far simpler to address, and the routing of the electrical control lines becomes trivial. In fact, there are already several recent demonstrations of 1D SLMs exploiting free-carrier dispersion effects [6,10]. We note that, while 1D SLMs are not inherently faster, the ease of routing and architectural simplicity can enable faster modulation effects to be used. Unfortunately, 1D beam shaping is far less versatile than 2D wavefront modulation. An attractive solution will be to map a 1D array of N^2 phase shifters to a 2D array of $N \times N$ pixels, which will enable 2D wavefront modulation bypassing the difficulty in routing the electrical control signals. To support this, a recent work [11] used a random medium to enable a 1D-to-2D mapping for imaging: a high-speed (~ 350 kHz) 1D mechanically-actuated SLM is used to focus light in a 2D plane through a random medium. However, arbitrary wavefront shaping in two dimensions was not demonstrated.

In this Letter, we propose a method to control a 2D wavefront by modulating the pixels physically arranged in a 1D array. The key is an inverse-designed phase-mask doublet, which maps

an input point source to a 2D spatial field profile that forms an orthogonal 2D intensity basis. Thus, an effective 2D SLM can be realized using a 1D SLM. Figure 1 shows the proposed optical architecture for the 1D-to-2D mapped SLM. The laser light is modulated using a 1D array of tunable pixels, which then passes through the composite phase masks. We design these two phase masks to route the light from each 1D pixel to produce a desired 2D intensity distribution at a specific plane (here the plane of the camera).

We first construct a forward model that simulates the light propagation from a 1D SLM through the free space and include the light's interaction with discretized phase masks. The phase masks span an area of 2 mm × 2 mm with 400 × 400 equally spaced elements. This leads to an element spacing of 5 μm. We employ the band-limited angular spectrum method to simulate the forward propagation [12], as shown below:

$$E(x, y, z_0) = E(x, y, 0) * h(x, y, z_o),$$

$$\mathcal{F}\{h(x, y, z_o)\} = e^{j\frac{2\pi}{\lambda}z_0\sqrt{1-(\lambda f_x)^2-(\lambda f_y)^2}} \times A(f_x, f_y).$$

$E(x, y, z)$ is the electric phasor field, $h(x, y, z)$ is the point spread function, $\mathcal{F}$ is the 2D spatial Fourier transform operator, λ is the wavelength of light, and z_0 is the propagation distance. The input source field is $E(x, y, 0)$. $A(f_x, f_y)$ is a mask that limits the spatial bandwidth to be lower than f_x and f_y, which blocks high-angle wavevector components that would otherwise wrap around and re-enter the simulation domain [12]. The effect of the phase mask is modeled by a point-by-point multiplication of the input field with the phase mask's complex amplitudes.

This forward model is then used in an automatic differentiation-based optimization method to design the phase profiles which will map the 1D pixel array to the 2D wavefront. For the optimization, we construct a cost function C based on the desired input–output mapping:
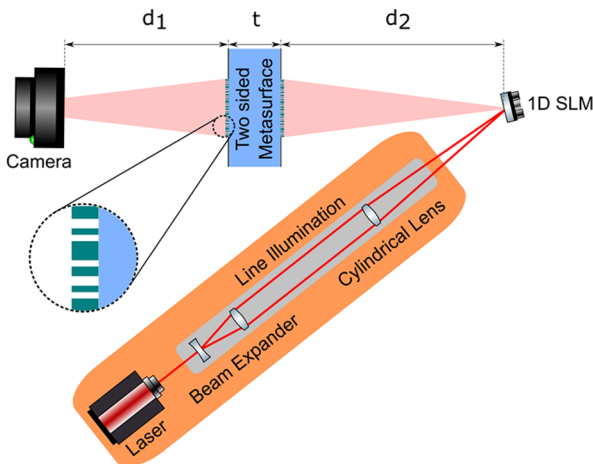
Fig. 1. Proposed optical architecture for using a 1D SLM for 2D wavefront shaping. Coherent light is focused into a line to efficiently illuminate a linear array of pixels (1D SLM). The modulated light is sent to a pair of meta-optical structures. After passing through the meta-optics doublet, the light is captured in a camera, where the arbitrary 2D patterns are observed. The gap between the 1D SLM and the first phase mask is kept at $d_2 = 2$ mm. The separation between two masks is $t = 1$ mm, corresponding to a standard glass wafer thickness so that masks can be fabricated on either side of a substrate [11]. The distance between the final mask and the camera is $d_1 = 2$ cm.
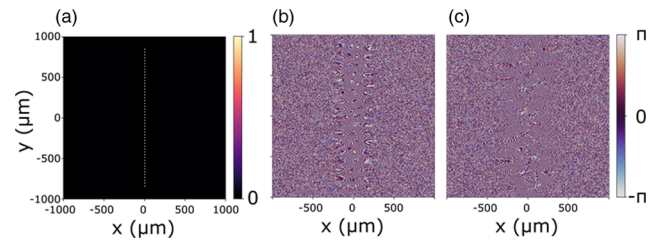
Fig. 2. (a) Input pixel intensity; optimized phase profiles for the (b) first and (c) second phase mask.

$$C = -\prod_{k}^{N}\left(\sum_{i,j} y_k^{(i,j)} \hat{y}_k^{(i,j)}\right),$$

where $y_k^{(i,j)}$ and $\hat{y}_k^{(i,j)}$ are the target and the output spatial distributions, respectively, for the kth input mode (in this case each pixel in the 1D array). N is the number of pixels in the 1D array. The 2D field is discretized in the (x, y) plane with i and j being the discretization indices. This cost function is designed to make the output modes similar to the desired modes, while ensuring that each output mode contains similar power.

The equation describing the cost function is represented as an acyclic, directed graph where nodes with children are mathematical operators that have a defined derivative, such as multiplication, addition, reduce sum, and discrete Fourier transform, while childless nodes are either variables or constants. The operator nodes take their children as arguments. The children of operators can be other operators, variables, and constants. Since the operators that are used are differentiable, the chain rule allows us to find the derivative of a node by calculating and combining the derivatives and values of its children in a process called automatic differentiation. Complete gradients of the cost function are calculated with respect to each phase-mask element and are updated using an optimization algorithm to minimize the value of the cost function. This representation is facilitated by the graph-based linear algebra library TensorFlow [13]. The phases are updated using the Adam optimizer [14].

Figures 2(b) and 2(c) show optimized phase masks for 1D-to-2D mapping. We impose a square aperture for the phase masks with dimensions of 2 mm × 2 mm. The 1D SLM pixel pitch is $p = 25$ μm.

Using these phase masks, we can map a 1D array to a 2D field distribution. When excited by individual pixels from the 1D SLM, the output field at the 2D SLM output will be illuminated. The output fields are well defined within the output pixel boundary. It is important to note that the output modes demonstrated in this Letter are just a single choice of basis, and other more appropriate bases can be used depending on the application.

Figure 3(a) shows the 1D array of 49 spots. Each spot maps to a specific point in the 2D plane, as shown in the 7 × 7 array in Fig. 3(b), when passing through two phase masks. The 49 points in the resulting 2D array will approximate a complete intensity basis in the 7 × 7 output space. The mean input-to-output power efficiency was 0.88 for all modes with a variance of 0.003. We note that the choice of 49 pixels is limited by the currently available computational resources in our team. More pixels can be added to increase the image resolution. We also emphasize that 1D SLMs with millions of pixels can be fabricated using current semiconductor technologies to the required resolution.
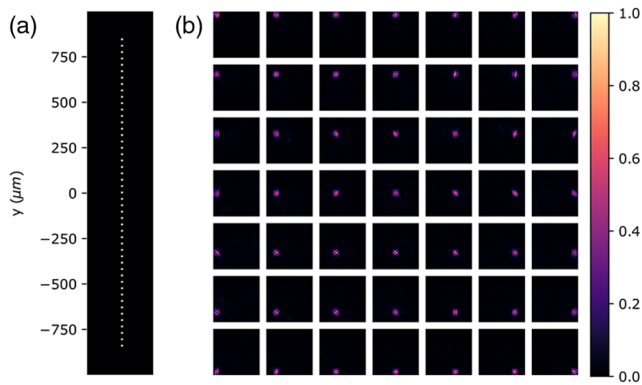
Fig. 3. (a) Input 49 element 1D SLM with all input pixels illuminated and (b) simulated output modes for 1D 49 element SLM input.
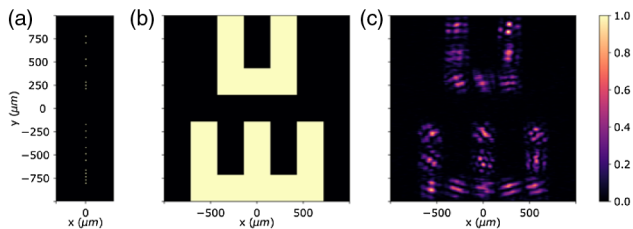

Fig. 4. (a) 1D SLM input field, (b) target output field, and (c) simulated output field using 1D-to-2D mapping.

However, the pitch of the input 1D SLM will eventually be limited by diffraction, as explained later in the Letter.

Illuminating appropriate pixels in the 1D array, arbitrary 2D patterns can be generated. Figure 4 shows the projection of such an arbitrary pattern: the letters "UW." We attribute the stripe-like features in the simulated output field to our choice of the cost function: our cost function does not prioritize uniformity inside a pixel, and rather optimizes the total power in that pixel.

Finally, we analyze how diffraction poses a limit on the proposed 1D-to-2D transformation. Light from different pixels in the 1D array impinges on the phase masks at different angles, and thus the reshaping of the 1D array to a 2D space fundamentally depends on the angular resolution of the phase-mask doublet. For the arrangements of the optics simulated here, the Abbe diffraction limit dictates that two points in the 1D SLM plane can be distinguished if their separation is greater than 633 nm (presuming a circular aperture). We hypothesize that when the pixel pitch approaches this limit, our 1D-to-2D mapping starts to fail. To validate this hypothesis, we modify the simulation so that the grid pitch is near the diffraction limit, without incurring high computational cost and memory requirement. Specifically, we reduce the size of the apertures (e.g., diameter of the meta-optics and lateral size of the 1D SLM) by a factor of 10, but keep the longitudinal distances the same. In this reduced simulation space, the Abbe diffraction limit becomes 6.33 μm, as only the aperture is scaled, and not the longitudinal dimensions. Then we optimize a set of identical systems (albeit with different pixel pitches in the 1D SLM) that map a four-pixel, 1D SLM to a 2×2 2D pixel output and quantify the error as the cumulative crosstalk (Fig. 5). A crosstalk of 1 indicates that energy from a single input pixel is distributed uniformly across all output pixels, while a crosstalk of 0 means that all power is within the intended output pixel. This value
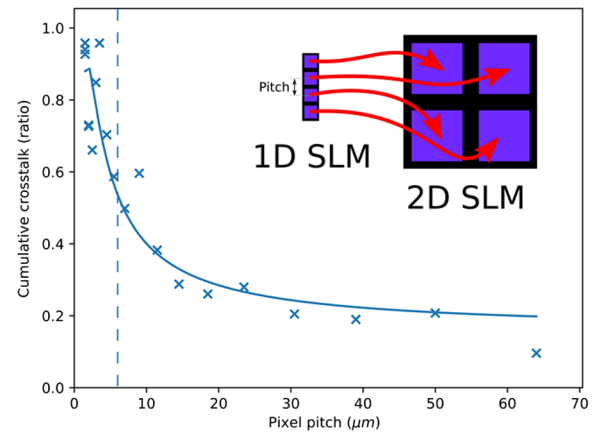
Fig. 5. Cumulative crosstalk between output modes for a range of trained systems that map a four-pixel 1D SLM to a 2×2 output SLM. The simulation region was shrunk by a factor of 10 to clearly observe the breakdown of our proposed method. All other simulation parameters are identical to the featured model, except for the input pixel pitch. The solid curve serves as a guide to the eye.

is summed across all the inputs for a given simulation to calculate the cumulative crosstalk. As expected, the performance of the phase-mask doublet markedly decreases as the input pixel separation approaches the diffraction limit (~6.33 μm). We note that the tolerable value of the crosstalk will depend on the exact application. Additionally, we anticipate the crosstalk effect primarily coming from the neighboring pixels; hence, the 2×2 simulation provides a good estimate of the crosstalk for larger arrays.

The proposed method could be experimentally verified with commercial SLMs, for example a grating light valve used by others [11]. In fact, the dimensions used in our simulations are motivated by experimental feasibility, such as the dimensions of the beam expanders and spacing between optics. The phase masks can be implemented using meta-optics [15]. Meta-optics are sub-wavelength diffractive optics that can shape the phase of incident light with high spatial resolution [16,17]. Sub-wavelength optical scatterers are spatially arranged in a meta-optic to provide spatially varying phase shifts to the incident optical wavefront [18–21]. The phasor response of the phase-mask elements can be simulated using a rigorous full-wave electromagnetic simulation, such as finite-difference time-domain or rigorous coupled-wave analysis [16,22]. Under local phase approximation (assuming the neighboring scatterers have minimal coupling), individual scatterers are placed where their phase delay matches the desired phase delay of the phase mask. The doublet can be realized by fabricating two meta-optics on both sides of a glass slide [23]. Additionally, millimeter-aperture, visible wavelength metasurfaces have already been reported and can potentially be scaled to even larger apertures [24].

In summary, we propose a method to generate arbitrary 2D intensity profiles from a 1D SLM using a pair of inverse-designed meta-optics. We validate our design via numerical simulation and explore how diffraction limits such mapping. Our proposed method can potentially alleviate the routing challenges for sub-wavelength SLMs, enabling a high-speed modulation of 2D optical modes.

All the simulations were performed on a Nvidia 1070Ti 8 GB, Intel i5-4690 CPU 3.5 GHz four-core, 8 GB system memory.

Disclosures. The authors declare no conflicts of interest.

Data Availability. Data underlying the results presented in this paper are not publicly available at this time but may be obtained from the authors upon reasonable request.

REFERENCES

1. G. W. Y. Peng, S. Choi, and N. Padmanaban, ACM Trans. Graph. **39**, 1 (2020).
2. D. Faccio, Opt. Photonics News **30**, 36 (2019).
3. X. Lin, Y. Rivenson, N. T. Yardimci, M. Veli, Y. Luo, M. Jarrahi, and A. Ozcan, Science **361**, 1004 (2018).
4. A. Ryou, J. Whitehead, M. Zhelyeznyakov, P. Anderson, C. Keskin, M. Bajcsy, and A. Majumdar, Photonics Res. **9**, B128 (2021).
5. A. P. Mosk, A. Lagendijk, G. Lerosey, and M. Fink, Nat. Photonics **6**, 283 (2012).
6. J. Park, B. G. Jeong, S. I. Kim, D. Lee, J. Kim, C. Shin, C. B. Lee, T. Otsuka, J. Kyoung, S. Kim, K.-Y. Yang, Y.-Y. Park, J. Lee, I. Hwang, J. Jang, S. H. Song, M. L. Brongersma, K. Ha, S.-W. Hwang, H. Choo, and B. L. Choi, Nat. Nanotechnol. **16**, 69 (2020).
7. A. Karvounis, V. V. Vogler-Neuling, F. U. Richter, E. Dénervaud, M. Timofeeva, and R. Grange, Adv. Opt. Mater. **8**, 2000623 (2020).
8. K. Liu, S. Sun, A. Majumdar, and V. J. Sorger, Sci. Rep. **6**, 37419 (2016).
9. B. J. Lechner, F. J. Marlowe, E. O. Nester, and J. Tults, Proc. IEEE **59**, 1566 (1971).
10. G. K. Shirmanesh, R. Sokhoyan, P. C. Wu, and H. A. Atwater, ACS Nano **14**, 6912 (2020).
11. O. Tzang, E. Niv, S. Singh, S. Labouesse, G. Myatt, and R. Piestun, Nat. Photonics **13**, 788 (2019).
12. K. Matsushima and T. Shimobaba, Opt. Express **17**, 19662 (2009).
13. M. Abadi, A. Agarwal, P. Barham, E. Brevdo, Z. Chen, C. Citro, G. S. Corrado, A. Davis, J. Dean, M. Devin, S. Ghemawat, I. Goodfellow, A. Harp, G. Irving, M. Isard, Y. Jia, R. Jozefowicz, L. Kaiser, M. Kudlur, J. Levenberg, D. Mané, R. Monga, S. Moore, D. Murray, C. Olah, M. Schuster, J. Shlens, B. Steiner, I. Sutskever, K. Talwar, P. Tucker, V. Vanhoucke, V. Vasudevan, F. Viégas, O. Vinyals, P. Warden, M. Wattenberg, M. Wicke, Y. Yu, and X. Zheng, "TensorFlow: Large-Scale Machine Learning on Heterogeneous Distributed Systems" (2015).
14. D. P. Kingma and J. Ba, "Adam: A Method for Stochastic Optimization," arXiv:1412.6980 (2017).
15. A. Zhan, S. Colburn, C. M. Dodson, and A. Majumdar, Sci. Rep. **7**, 1673 (2017).
16. A. Zhan, S. Colburn, R. Trivedi, T. K. Fryett, C. M. Dodson, and A. Majumdar, ACS Photonics **3**, 209 (2016).
17. S. M. Kamali, E. Arbabi, A. Arbabi, and A. Faraon, Nanophotonics **7**, 1041 (2018).
18. H. Kwon, E. Arbabi, S. M. Kamali, M. Faraji-Dana, and A. Faraon, Nat. Photonics **14**, 109 (2020).
19. D. Lin, P. Fan, E. Hasman, and M. L. Brongersma, Science **345**, 298 (2014).
20. N. Yu and F. Capasso, Nat. Mater. **13**, 139 (2014).
21. E. Tseng, S. Colburn, J. Whitehead, L. Huang, S.-H. Baek, A. Majumdar, and F. Heide, "Neural Nano-Optics for High-quality Thin Lens Imaging," arXiv:2102.11579 (2021).
22. V. Liu and S. Fan, Comput. Phys. Commun. **183**, 2233 (2012).
23. A. Arbabi, E. Arbabi, S. M. Kamali, Y. Horie, S. Han, and A. Faraon, Nat. Commun. **7**, 13682 (2016).
24. S. Colburn, A. Zhan, and A. Majumdar, Optica **5**, 825 (2018).